Tight junctions negatively regulate mechanical forces applied to adherens junctions in vertebrate epithelial tissue

Guillaume Hatte, Claude Prigent, Jean-Pierre Tassan

Tight junctions negatively regulate mechanical forces applied to adherens junctions in vertebrate epithelial tissue

Guillaume Hatte[1,2], Claude Prigent[1,2] and Jean-Pierre Tassan[1,2,3]

1 - CNRS UMR 6290, Rennes, France

2 - Université de Rennes 1, Institut de Génétique et Développement de Rennes, Rennes, France

Address : IGDR, UMR 6290 CNRS Université de Rennes 1, 2 avenue du Professeur Léon Bernard, 35043 Rennes Cedex, France.

3 - Corresponding author: jean-pierre.tassan@univ-rennes1.fr

Key words: biosensor/cadherin/cytokinesis/epithelium/apical junctions

Summary statement

Using a FRET tension biosensor, we show that tight junctions negatively regulate mechanical forces applied to adherens junctions. This regulation becomes essential when junctions are put under stress such as cytokinesis.

Abstract

Epithelia are layers of polarised cells tightly bound to each other by adhesive contacts. Epithelia act as barriers between an organism and its external environment. Understanding how epithelia maintain their essential integrity while remaining sufficiently plastic to allow events such as cytokinesis to take place is a key biological problem. In vertebrates, the remodelling and reinforcement of adherens junctions maintains epithelial integrity during cytokinesis. The involvement of tight junctions in cell division, however, has remained unexplored. Here, we examine the role of tight junctions during cytokinesis in the epithelium of the *Xenopus laevis* embryo. Depletion of tight junction-associated proteins ZO-1 and GEF-H1 leads to altered cytokinesis duration and contractile ring geometry. Using a tension biosensor, we show that cytokinesis defects originate from misregulation of tensile forces applied to adherens junctions. Our results reveal that tight junctions regulate mechanical tension applied to adherens junctions, which in turn impacts cytokinesis.

Keywords: epithelium, tight junctions, adherens junctions, ZO-1, GEF-H1, mechanotransduction, Xenopus laevis, cytokinesis

Introduction

Found in all metazoans, epithelia represent a basic type of cell organisation, and are required to ensure the physical cohesion necessary to form tissues and organs. By acting as mechanical and chemical barriers, epithelia constitute vital fences between different tissue compartments, allowing polarised absorption and secretion. Epithelia comprise polarised cells, which maintain strong cell-cell contacts to guarantee the integrity indispensable for barrier functions. At their apical side, epithelial cells develop a junctional complex, formed by adherens and tight junctions, which seals cell-cell contacts. Adherens junctions provide mechanical attachments between neighbouring cells (Lecuit and Yap, 2015). These junctions are composed of cadherin, a transmembrane protein whose extracellular domain creates homophilic interactions with cadherin of neighbouring cells. Cadherin indirectly links the actin cytoskeleton, *via* association of α and β catenins to its intracytoplasmic tail (Leckband and de Rooij, 2014). In vertebrates, tight junctions (Zonula Occludens, ZO) are the most apical junctions. They act as regulators of transepithelial permeability, intramembrane barriers and signalling platforms (Citi et al., 2014). Tight junctions are composed of a variety of transmembrane proteins, such as claudins and occludin, which are connected intracytoplasmically to the actin cytoskeleton *via* ZO proteins.

Although epithelia maintain strong cell-cell contacts, which guarantee the integrity indispensable for barrier functions, they also keep plasticity, which is crucial during development and morphogenesis. Morphogenesis relies on diverse cellular events, including division, intercalation and extrusion, all of which depend on the contractility of the actomyosin cytoskeleton. During tissue remodelling, which occurs during development and morphogenesis, cell-cell contacts are maintained, thus preserving tissue integrity. This requires that adherens junctions and mechanical forces produced by the actomyosin cytoskeleton are intimately linked (Herszterg et al., 2013). Maintaining epithelial plasticity and integrity is also vital throughout adult life, during which epithelia are constantly remodelled or regenerated by cell proliferation. How epithelia remain plastic while simultaneously maintaining their integrity is a key question. To decipher this problem, it is vital to investigate the regulation of mechanical forces produced by the actomyosin cytoskeleton at adherens junctions.

Cell division in epithelia provides a physiological model for studying such antagonistic constraints between cell-cell contacts maintenance and plasticity. Indeed, during cytokinesis, cell-cell contacts are challenged by drastic shape changes, both of the dividing cell and of its neighbours, which resist division (Founounou et al., 2013). During cell division, a contractile actomyosin ring causes ingression of the plasma membrane and the associated cytoskeleton cortex, thus allowing separation of the two daughter cells. The contractile actomyosin ring triggers the reinforcement of adherens junctions, thus explaining how these junctions counteract the cytokinetic ring constriction and contribute to maintenance of epithelial integrity (Higashi et al., 2016). However, the main question of how the cytokinetic actomyosin ring overcomes the resistance of neighbouring cells, ultimately allowing cytokinesis progression, remains unanswered.

In *Drosophila*, the contractile ring is anchored at the adherens junctions (Guillot and Lecuit, 2013). This led to the hypothesis that constriction of the cytokinetic ring would induce variation of tensile forces applied on adherens junctions. Recently, we used a cadherin tension biosensor to investigate how mechanical forces acting at adherens junctions are regulated during cell division in the epithelium of *Xenopus* embryos (Herbomel et al., 2017). Using this approach, we have shown that the epithelium is under stable tension. In addition, mechanical tension across cadherin is similar in dividing and non-dividing epithelial cells, indicating either that variations of tensile force applied on cadherin are modest, or that adherens junctions are not the sites where mechanical forces vary. This suggests that other factors that remain to be identified are involved in the regulation of mechanical tension applied at the adherens junctions.

Because adherens junctions are main sites where mechanical forces apply, their role during cell division is a key focus of previous studies, particularly in *Drosophila* (Founounou et al., 2013; Guillot and Lecuit, 2013; Herszterg et al., 2013; Morais-de-Sá and Sunkel, 2013). In contrast, the involvement of tight junctions has remained unexplored. Here, we investigate the involvement of two tight junction-associated proteins, ZO-1 and GEF-H1 in the regulation of mechanical forces applied on adherens junctions and their involvement in cytokinesis in the epithelium of the *Xenopus* embryo. Our results provide

insight into the role of tight junctions in the negative regulation of mechanical forces applied to adherens junctions necessary for cytokinesis to occur.

Results

Tight junctions are essential for cytokinesis

To investigate the possible role of tight junctions during epithelial cell cytokinesis, we knocked down the two tight junction-associated proteins ZO-1 and GEF-H1. ZO-1 (zonula occludens-1) (Stevenson et al., 1986) is a core tight junction protein, which acts as a scaffold linking tight junction transmembrane proteins, such as occludin (Furuse et al., 1994), with the actin cytoskeleton (Fanning et al., 1998). GEF-H1 (guanine nucleotide exchange factor H1) is a component of tight junctions (Benais-Pont et al., 2003) which exhibits RhoA small GTPase activity (Aijaz et al., 2005). It regulates tight junctions (Benais-Pont et al., 2003) and is involved in apical constriction, which contributes to morphogenetic movements, leading to neural tube closure (Itoh et al., 2014).

To knockdown ZO-1 and GEF-H1, we used two antisense morpholino (Mo) oligonucleotides, which decrease ZO-1 and GEF-H1 levels in Xenopus embryo (supplementary material Fig. S1 and Itoh et al., 2014). At the gastrula stage, these two proteins were depleted to about half (54.6 ± 0.6 % in Mo ZO-1 treated cells and 47.7 ± 2.7 % in Mo GEF-H1 treated cells) compared to untreated cells (Fig. 1A). We observed cell division failures in ZO-1 and GEF-H1 depleted cells of living embryos, (Fig. 1B and C). This was correlated to the presence of multinucleated cells (Fig. 1D). Taken together, our results suggested that ZO-1 and GEF-H1 depletions induce cytokinesis defects. Although most embryos injected with ZO-1 antisens morpholinos were affected (proportion of embryos exhibiting multinucleated cells: control 4.5 % of embryos analysed, Mo ZO-1 79.6 % and Mo ZO-1 + ZO-1-GFP 17.4 %), numerous cells exhibited one nucleus indicating that they divided correctly (Fig. 1D). Moreover, these depletions did not detectably alter the overall structure of the epithelium (Fig. 1A), allowing further analysis.

Depletion of ZO-1 and GEF-H1 alter cytokinesis duration and contractile ring geometry

To analyse the effect of ZO-1 and GEF-H1 depletions during cytokinesis, constriction of the actomyosin contractile ring was followed *in vivo* in *Xenopus* gastrulae using actin fluorescent probes. At this developmental stage, epithelial cells divide by asymmetric furrowing from the basal side towards the apical pole (Le Page et al., 2011). Apical cell-cell contacts were deformed at the division site (Fig. 2A, arrowheads in control 180 s). As constriction advanced, the contractile ring adopted an ovoid shape (Fig. 2A, side view, 360 s). In ZO-1 and GEF-H1 depleted cells, the basal-to-apical asymmetric furrowing was maintained (Fig. 2A, Mo ZO-1 and Mo GEF-H1). However, the contractile ring was flattened (Fig. 2A, side views, 300 s) with a Ring Shape Index (R.S.I., the ratio between ring length and height, R.S.I.=1 being a circle) significantly higher in Mo ZO-1 (R.S.I.= 4.7 ± 0.2 (mean ± s.e.m.)) and Mo GEF-H1 (3.8 ± 0.2) compared to controls (2.1 ± 0.1) (Fig. 2B). Moreover, apical constriction of the ring was significantly slower in depleted cells (Mo ZO-1: 648 ± 45.1 s, 21 out of 21 recorded cells, Mo GEF-H1: 538.3 ± 27.6 s, 13/22 cells) than in controls (377.5 ± 11.4 s, 46/46 cells) (Fig. 2C). Expression of ZO-1-GFP in Mo ZO-1 or GEF-H1 in Mo GEF-H1 knockdown embryos restored both the cytokinesis duration and the ring shape (Fig. 2A, B and C).

Altogether, our results indicate that ZO-1 and GEF-H1 are required for epithelial cell cytokinesis. Moreover, defects induced by ZO-1 and GEF-H1 depletion evoked increased cell-cell junctions resistance to cell division, which might result from increased mechanical forces applied to cell-cell junctions (Founounou et al., 2013; Guillot and Lecuit, 2013).

Tight junctions regulate tension applied to adherens junction.

Because adherens junctions that link neighbouring cell membranes and their internal actin cytoskeletons are the main sites affected when mechanical forces are applied, we focused on these junctions. Although levels of C-cadherin (also termed EP-cadherin), the main adherens-junctions molecule of the Xenopus gastrula (Choi et al., 1990; Ginsberg et al., 1991), and β-catenin, which links cadherin with α–catenin, were reduced in ZO-1 and GEF-H1 depleted cells, the perijunctional actin filaments (F-actin) were significantly

increased in GEF-H1 depleted cells compared to control cells (Fig. 3A, 192.5 ± 11.6 %) and slightly increased in ZO-1 depleted cells (Fig. 3A, respectively 130.6 ± 12.2 %). As shown previously (Nandadasa et al., 2012), depletion of α-catenin, which indirectly links C-cadherin to the actomyosin cytoskeleton also led to a significant decrease of C-cadherin (Fig. 4A). However, in contrast to ZO-1 and GEF-H1 depletions, α-catenin depletion induced a significant reduction of perijunctional F-actin without altering the cytokinesis duration and the contractile ring shape (Fig. 4A, B, C). These results suggested that the flattened-shape contractile ring and the increased cytokinesis duration in ZO-1 and GEF-H1 depleted cells could result from the increase of F-actin perijunctional cytoskeleton. We hypothesized that the reinforcement of the perijunctional F-actin might induce an increase of the tensile force applied to adherens junctions. To test this assumption, we used CcadTSMod, a FRET tension sensing probe. It consists in a tensile force sensitive module (TSMod) integrated into the cytosolic domain of C-cadherin (Herbomel et al., 2017) (Fig. 3B). We have previously shown that this tension probe detects tensile force variations on adherens junctions in Xenopus embryo. Whereas in control cells the CcadTSMod mean fluorescence lifetime measured on entire fields of acquisition (10 cells per field) was 2596.9 ± 11.6 ps, it significantly increased to 2662.9 ± 16.5 ps and 2660.3 ± 14.4 ps in ZO-1 and GEF-H1 depleted cells, respectively (Fig. 3C). As a control, we used a construct without the cytosolic domain (CcadTL) which is not linked to the actomyosin cytoskeleton. Therefore, it is not submitted to mechanical forces and exhibits the minimum fluorescence lifetime (Borghi et al., 2012). CcadTL fluorescence lifetime was similar in control, ZO-1 and GEF-H1 depleted cells (respectively 2483.8 ± 7.6 ps, 2480.7 ± 6.1 ps and 2484.1 ± 4.2 ps, Fig. 3C). Correlated with the reduction of perijunctional F-actin (Fig. 4A), the CcadTSMod fluorescence lifetime was significantly decreased in α-catenin depleted cells compared to controls (2544.2 ± 5.0 ps versus 2604.8 ± 6.9 ps) (Fig. 4C). These results indicated an increase in global tensile forces applied to adherens junctions induced by ZO-1 and GEF-H1 depletions. This led us to hypothesise that the increase in tensile forces may cause cytokinesis defects induced by ZO-1 and GEF-H1 depletions.

Increased tensile forces applied on adherens junction alters contractile ring geometry and cytokinesis

To test a potential relationship between increased forces and the cytokinetic defects induced by ZO-1 and GEF-H1 depletions, we increased tensile forces applied to adherens junctions by incubating embryos in 2'-deoxyadenosine 5-triphosphate (dATP), which stimulates contractility (Regnier et al., 2000). Under these conditions, tensions applied to adherens junctions, perijunctional F-actin recruitment and Ring Shape Index (R.S.I.) were significantly increased compared to control cells (Fig. 5A,B,C,D), thus mimicking ZO-1 and GEF-H1 depletions. Thus, increased tensile forces applied to adherens junctions correlated with ring geometry defect. To further challenge a causal relationship between increased forces on adherens junctions and cytokinetic defects, we took advantage of a vinculin deletion mutant (VinD1) recently developed (Higashi et al., 2016), which decreases vinculin recruitment. Vinculin is an F-actin binding protein recruited at the adherens junction by a tension-induced conformational change of α-catenin (Yonemura et al., 2010) leading to adherens junctions reinforcement. VinD1 expression significantly decreased cytokinesis duration, as reported previously (Higashi et al., 2016), modestly increased R.S.I., and did not significantly affect the CcadTSMod fluorescence lifetime (Fig. 5F,G,H). The absence of effect on the tensile forces could be explained by the fact that in Xenopus epithelium tensile forces applied on cadherin at the adherens junctions are at equilibrium; they are approximately 3 pN (Herbomel et al., 2017), which is below the 5 pN required to unfold α-catenin and recruit vinculin (Yao et al., 2014). Expression of VinD1 suppressed ring shape defect (Fig. 5E,F, R.S.I. = 4.6 ± 0.3 for Mo ZO-1 and 2.3 ± 0.1 for Mo ZO-1+VinD1 compared to 2.0 ± 0.1 in controls,), cytokinesis duration defect (Fig. 5G, 741 ± 55 s for Mo ZO-1 and 378 ± 18 s for Mo ZO-1+VinD1 compared to 393 ± 17 s in controls) and increased tensile forces (mean fluorescence lifetime, Fig. 5H) induced by ZO-1 depletion. Taken together, these results indicate that in ZO-1 and GEF-H1 depleted cells, a global increase of tensile forces applied to cadherin enhance the resistance of apical junctions to cytokinesis, which ultimately affects the contractile ring geometry and the cytokinesis duration. They also indicate that tight junction-associated proteins ZO-1 and GEF-H1 are implicated in the negative regulation of global tensile force applied to adherens junctions.

GEF-H1 could act by regulating membrane trafficking *via* the exocyst complex.

Next, we investigated how GEF-H1 regulates tensile forces applied on adherens junctions. Recently, GEF-H1 has been shown to regulate assembly and localization of the exocyst (Pathak et al., 2012). Exocyst is a multiprotein complex which plays a crucial role in tethering and fusion of vesicles at the plasma membrane (Wu and Guo, 2015). This regulation requires GEF-H1 GTP exchange activity and interaction of GEF-H1 with the Sec5 subunit of the exocyst complex (Pathak et al., 2012). To test if exocyst regulation by GEF-H1 could be involved in tensile forces regulation applied on adherens junctions, we expressed the inactive GEF-H1^{Y384A} mutant (Itoh et al., 2014; Krendel et al., 2002) or GEF-H1$^{(aa\ 108\text{-}226)}$, the GEF-H1 domain which links Sec5 and acts as a competing peptide (Pathak et al., 2012). Fluorescence lifetime of CcadTSMod increased in cells expressing GEF-H1^{Y384A} and GEF-H1$^{(aa\ 108\text{-}226)}$ mutants compared to controls (Fig. 6A, respectively 2653.4 ± 7.8 ps and 2635 ± 4.7 ps ; control 2599.4 ± 6.9 psec). Moreover, cells expressing GEF-H1 Y^{384A} or GEF-H1$^{(aa\ 108\text{-}226)}$ also exhibited the contractile ring apical constriction defect (Fig. 6B,C). Similarly to GEF-H1 depletion, expression of GEF-H1 Y^{384A} or GEF-H1$^{(aa\ 108\text{-}226)}$ led to decreased C-cadherin (Fig. 6D) and β-catenin levels (supplementary material Fig. S3). Taken together, these results suggest that GEF-H1 dependent regulation of the exocyst may participate in the negative regulation of tensile force applied on the adherens junctions. As ZO-1 depletion affects GEF-H1 levels (Fig. 1A), it could be possible that the effect on force applied on adherens junction could occur *via* GEF-H1 dependent regulation of the exocyst. Further studies will be necessary to explore the involvement of GEF-H1-dependent exocyst regulation in the control of forces applied on adherens junctions.

Discussion

In summary, our results reveal that the tight junction-associated proteins ZO-1 and GEF-H1 are involved in negative regulation of mechanical forces applied to adherens junctions necessary for cytokinesis completion in the epithelium of Xenopus embryo.

Constriction of the cytokinetic actomyosin ring triggers adherens and tight junctions reinforcement (Higashi et al., 2016). This reinforcement was proposed to participate in the maintenance of the epithelium integrity during cell division. However, it remained unclear how the contractile ring ultimately wins the 'tug of war' against apical junctions, allowing cytokinesis progression. In the present study, measurement of tensile forces

applied to C-cadherin molecules showed that tight junction-associated proteins ZO-1 and GEF-H1 are involved in the regulation of mechanical forces applied to adherens junctions. Our results are in agreement with those obtained in cultured epithelial cells, which show that ZO-1 depletion increases intercellular tensions (Bazellières et al., 2015), and that ZO-1 ZO-2 double depletion increases contractility of the perijunctional actomyosin associated with the adherens junctions (Choi et al., 2016; Fanning et al., 2012). In contrast, in endothelial cells cultured *in vitro*, ZO-1 depletion decreases tensile forces applied to VE-cadherin (Tornavaca et al., 2015). This discrepancy may lie in the cell types studied, epithelial versus endothelial, which display different apical junction's organizations (Dejana et al., 2009). Nevertheless, our results support a model in which ZO-1 and GEF-H1 regulate apical cell-cell contacts resistance to the contractile ring constriction. Owing to cell-cell contacts and the mechanical coupling between epithelial cells (Twiss and de Rooij, 2013), the cell shape modifications of the dividing cell deform neighbouring cells thereby producing a mechanical stress (Bosveld et al., 2016; Founounou et al., 2013; Herszterg et al., 2013). GEF-H1 was previously shown to be involved in mechanotransduction (Guilluy et al., 2011). Upon mechanical stimuli, GEF-H1 activates Rho GTPase and promotes cellular stiffness. In epithelial cells, GEF-H1 is inhibited by junctional recruitment (Aijaz et al., 2005) suggesting a potential signalling role of this protein. We speculate that during cytokinesis, GEF-H1 inhibition might be suppressed by mechanical stress produced by the dividing cell allowing the cell-cell contacts adaptation necessary for cell division (Fig. 6E). In our model, active GEF-H1 released from junctional inhibition would activate, *via* RhoA GTPase, actomyosin contraction at the level of tight junctions. This would lead to an increase inhibition by tight junctions of forces applied on adherens junctions. Further studies will be necessary to understand how tight junctions sense and regulate mechanical forces applied on adherens junctions.

In this study, we showed that ZO-1 and GEF-H1 depletions have different impact on C-cadherin, α- and β-catenin levels. However, the CcadTSMod mean fluorescence lifetimes are similar (Fig. 3C), suggesting that tensions reached a maximum. We hypothesize that ZO-1 depletion could induce a stronger and transient effect on tensile forces than GEF-H1 depletion. Increased tensile forces induced by ZO-1 depletion could reach a threshold value harmful for the epithelium integrity and functions. We propose that a compensatory mechanism activated by increased tensile forces induced by ZO-1 depletion would reduce

the amount of C-cadherin, α- and β-catenins at the adherent junctions which would limit the increase of tensile forces induced by ZO-1 depletion. Because tensile forces in GEF-H1 depleted cells would not reach the threshold value, the compensatory mechanism would not be activated. Compensatory mechanism acting at the apical junctional complex has already been described for ZO depleted cells treated with a ROCK inhibitor (Choi et al., 2016). Such a hypothetical mechanism would protect the epithelium against oversized forces, which might alter the epithelium integrity and functions when tight junctions are compromised. Further investigations will be required to understand the details of this mechanism.

It was previously shown that cytokinesis defects in cells mutated for the tumor suppressor gene p53 could lead to genomic instability and cancer (Fujiwara et al., 2005). Our results showing that altered tight junctions lead to misregulation of mechanical tensions on adherens junctions represents a previously unreported origin of cell division defects which might ultimately lead to cancer formation and progression.

Materials and methods

DNA constructs and morpholinos

pT7T-ZO-1-GFP (mouse) and pT7T-GEF-H1a^{Y384A} (Xenopus) were PCR amplified respectively from pCAGGS-ZO-1-GFP (Matsuda, 2004), pCS2-myc-GEF-H1-Y444A (a kind gift of Sergei Y. Sokol) (Itoh et al., 2014). pT7T-GEF-H1 WT and pT7T-GEF-H1$^{(aa\ 108\text{-}226)}$ were generated by PCR amplifying the corresponding sequences from Xenopus GEF-H1a obtained from Source Bioscience (clone image: 4173243). pT7T-VinD1 was obtained by amplification of the first 258 amino-acids of chicken vinculin (Grashoff et al., 2010). All PCR fragments were subcloned into the pT7T vector. pCS2-GFP-GPI (GFP-membrane) and pCS2-mRFP-GPI (RFP-membrane) plasmids were kindly provided by M. Brand (Dresden University of Technology, Germany), pCS2-mcherry-Utr-CH was a gift of W.M. Bement (Burkel et al., 2007), pCS2-life-act-GFP was a gift of U. Engel (Marx et al., 2013). For tension measurements, pT7T-CcadherinTSMod described previously (Herbomel et al., 2017) was used. The CcadherinTSMod contains the entire FRET tension module created by Grashoff et al. (2010) composed of an elastic linker interspaced between the fluorescence proteins mTFP1 and YFP integrated into the cytosolic cadherin domain. We have previously shown that CcadTSMod and EcadTSMod (Borghi et al., 2012) tension sensors exhibit similar fluorescence lifetimes in blastula embryo (Herbomel et al., 2017). This is also the case in gastrula embryos which we used in the present study (supplementary material Fig. S2). As a control, a construct without the cytosolic domain (CcadTL) was used. Because CcadTL is not linked to the actomyosin cytoskeleton, it is not submitted to mechanical forces and therefore exhibits the minimum fluorescence lifetime (Borghi et al., 2012). All plasmids were linearized and mRNAs were generated by *in vitro* transcription using the T7 or SP6 mMessage mMachine kit (Ambion).

For knockdown experiments, antisense morpholinos were produced by Gene Tools. For ZO-1 depletion, an antisense morpholino (5'-GCCGGTGTCAGTATGAGTCCCCAGA-3') has been designed to target the 5'UTR of the two genes encoding ZO-1. Previously described morpholinos targeting the 5'UTR of GEF-H1a (5'-AGGTGCGGTCAATGCCGGACATTGA-3') (Itoh et al., 2014) and the initiation codon for α-catenin (5'-ATGTTTCCTGTATTGAGAGTCATGC-3') (Nandadasa et al., 2012) were used. The standard morpholino (5'-CCTCTTACCTCAGTTACAATTTATA-3', Gene Tools) was used as control.

Preparation of Xenopus embryos and micro-injection

Xenopus laevis albinos were obtained from Biological Resources Centre (CRB, Rennes, France). All animal experiments were performed in accordance with the approved protocols and guidelines at Rennes 1 University by the Comité Rennais d'Ethique en Matière d'Expérimentation Animale (C2EA-07) and the French Ministry for Education and Research (3523813). Eggs were fertilized *in vitro* and embryos were collected as described previously (Hatte et al., 2014). After dejelling, embryos were placed in 5% of Ficoll in F1 medium (10 mM HEPES pH 7.6, 31.2 mM NaCl, 1.75 mM KCl, 59 µM MgCl2, 2 mM NaHCO3, and 0.25 mM CaCl2) for microinjection. mRNAs were microinjected into one blastomere of 4- or 8-cell stage embryos. For GEF-H1 knowdown experiments, 40 ng of morpholino in 13.8 nl were microinjected into one blastomere at the 4-cell stage, and for Mo ZO-1 and Mo α-catenin respectively 40 ng and 20 ng of morpholino in 9.2 nl were microinjected into one blastomere at 8-cell stage. mRNAs quantity injected were: GFP-membrane, 0.5 ng; RFP-membrane, 0.5 ng; life-act-GFP, 0.5 ng; mcherry-utr-ch, 0.5 ng; ZO-1-GFP, 2 ng; GEF-H1 WT, 0.25 ng; CcadTSMod, 2 ng; CcadTL, 2 ng; VinD1, 1 ng; GEF-H1^{Y384A}, 8 ng; and GEF-H1$^{(aa\ 108\text{-}226)}$, 8 ng. Embryos were then placed at 16°C overnight and analyzed at gastrula stage (stage 11, Nieuwkoop and Faber, 1967)

Indirect-immunofluorescence

Albino embryos were injected with membrane marker (GFP- or RFP- membrane) used as lineage tracers and with or without Mo GEF-H1, Mo ZO-1 or Mo α-catenin. Indirect immunofluorescence was performed as described previously (Hatte et al., 2014). Briefly, embryos were fixed with 2% trichloroacetic acid (TCA) in F1 1X. After embryos were devitellinated, cells were permeabilized in PBS + 1% Triton X-100 for 20 minutes at room temperature, incubated in PBS + 0.1% Triton X-100 (PBST 0.1%) for 10 minutes and then blocked 1 hour in 2% BSA in PBST 0.1% (BSA-PBST). Embryos were incubated overnight in BSA-PBST at 14°C with anti-GFP (Roche, clone 7.1 and 13.1, 11914460001, 1:100), anti-mCHERRY (abcam, Ab167453, 1:200), anti-ZO-1 (Zymed, 33-9100, 1:200), anti-GEF-H1 (Exalpha, Sheep lfc X1089P, 1:100), anti-C-cadherin (DHSB, 6B6, 1:200), anti-β-catenin (Santa cruz, H102:sc-7199, 1:100), anti-α-catenin (ThermoFisher Scientific, PA1-25081, 1:100) and anti-phospho S20 myosin light chain (S19 in Xenopus) (Abcam, ab2480, 1:100). After washing with PBST 0.1%, embryos were incubated with Alexa Fluor 488 or

555 anti-mouse, anti-rabbit or anti-sheep (ThermoFisher Scientific) and TO-PRO-3 to stain DNA (Invitrogen, 0.5 µg/ml) in BSA-PBST for 1 hour at room temperature. After washing with PBST 0.1%, embryos were mounted in Vectashield (Vector). For actin staining, embryos were fixed in 3.7% formaldehyde for 2 hours at room temperature, permeabilized and blocked as previously described. After blocking, embryos were incubated with Alexa 555-Phalloïdin (Life Technologies, 1:200= 1U/ml) and TO-PRO3 for 2 hours and mounted in Vectashield.

Western blot analysis

Proteins were extracted as previously described by Ann Miller lab (Reyes et al., 2014). Protein blot was incubated with anti-ZO-1 (Zymed, 33-9100, 1:500) and an anti-β-tubulin (TUB 2.1, sigma, 1:1000) antibodies. Secondary anti-mouse peroxidase-coupled immunoglobulins were from Jackson.

Treatment with dATP

Embryos at the 4-cell stage were microinjected with mRNA coding GFP-GPI (GFP-membrane) as described above. When they reached the gastrula stage, embryos were treated with 1 mM of dATP (Promega, U120D) in F1 1X during 20 minutes prior to imaging.

Confocal microscopy with living and fixed embryos

Living embryos were mounted as previously described (Hatte et al., 2014). Fixed and live imaging was performed using a Leica SP5 confocal microscope with 40x/1.25-0.75 HC PL APO (WD 0.1 mm) or 63X/1.4-0.6 HCX PL APO (WD 0.14 mm) oil immersion objective lens or a Leica SP8 confocal microscope with 40x/1.30 HC PL APO or 63x/1.4 HC PL APO oil immersion objective lens (Microscopy Rennes imaging Center, MRiC). For FLIM measurements, a FastFLIM microscope previously described (Leray et al., 2013) was used, a time lapse of 5 consecutive time frames was acquired for all the conditions.

Images processing and quantification

Images were processed using ImageJ software (Rasband, W.S., http://rsb.info.nih.gov/ij) and figures were prepared using ImageJ and Photoshop. Graphing was performed using R software and Microsoft Excel. In live experiments, only cells with one furrow showing no cytokinesis failure were analysed.

Quantification of immunolabelling at adherent and tight junctions. The mean fluorescence pixel intensity at cell-cell junctions was measured along a linear ROI placed at the maximum fluorescence plane. The mean fluorescence pixel intensity at proximity of cell-cell junctions was measured along a linear ROI with identical line size to ROI used for quantification at cell-cell junctions and subtracted to the pixel intensity at junction.

Cytokinesis timing and apical constriction measurement. The cytokinesis duration is the time during which the contractile ring contracts. To standardize measurements, the beginning and end of cytokinesis were respectively standardized as the time point just before F-actin started accumulating at the cleavage site and when the actomyosin contractile ring fully ingressed and concentrates at the apical pole of the cell.

Contractile ring shape. The ring shape index (R.S.I.) was calculated as the ratio between the length (parallel to the epithelium plane) and height (orthogonal to the plane of the epithelium) of the contractile ring. To avoid bias due to differences in the cytokinesis duration which could distort the ring shape index, measurements of the ring length were standardized: for all conditions they were done when the ring height reaches 4 µm.

FLIM measurements. All analyses were done as previously described (Herbomel et al., 2017). Briefly, the percentage of photobleaching was determined in a small area in the fluorescence image, if the decrease was superior to 10% between the first and the last time, the fields was not analysed. Then a mask corresponding to the FRET sensor or controls localized at cell junctions was created on fluorescence images and subsequently used to retrieve the fluorescence lifetime of this protein pool. One value represents the mean of the whole field values (10 cells per field), results are expressed in ps. Fire LUT was applied to fluorescence lifetime images.

Statistical analysis

No statistical method was used to predetermine sample size. The experiments were not randomized and investigators were not blinded to allocation during experiments and outcome assessment. Experiments were repeated at least two times. Sample sizes are precised for each experiment in figure legends. For each representative image, sample sizes (n) are indicated in the figure legend. A Shapiro-Wilk test was done for each group to determine the distribution normalities. Where appropriate, a two-tailed unpaired Student *t*-test was applied to determine statistical significance. In cases where variances were different, the unequal variance t-test was used. For groups not displaying a normal distribution, a Wilcoxon signed-rank test was done as indicated in figure legends. Statistical analysis was performed in R software.

Availability of materials

All materials generated in this study are freely available on request.

Acknowledgements

We are grateful to Malgorzata Kloc (The Houston Methodist Hospital, Houston TX, USA) Michael V. Danilchik (Oregon Health and Science University, Portland, OR, USA), Roland Le Borgne (IGDR, Rennes, France), Sarah Dixon (IGDR, Rennes, France) and former and present members of C. Prigent's team for helpful discussions and critical reading on the manuscript. We thank Marc Tramier, Gaëtan Herbomel and Claire Déméautis (IGDR, Rennes, France) for the CcadTSMod biosensor and help with the FastFLIM microscope and Yann Le Cunff (IGDR, Rennes, France) for helpful discussion with statistical analysis. We also thank the Microscopy Rennes Imaging Center (MRic, BIOSIT, IBiSA). We are grateful to all persons who provided us with plasmid constructions and Robert Rottapel for his help with anti-GEF-H1 antibodies. This work was supported by le Centre National de la Recherche Scientifique (CNRS), l'Agence Nationale de la Recherche (ANR, KinBioFRET), La Ligue Départementale contre le Cancer (comités 29 et 35). G.H. was supported by the MENESR and partly by a grant from the Ligue Nationale contre le Cancer.

Author contributions

G.H. carried out the experiments, generated and interpreted the data. J.-P.T. designed research and supervised the project. G.H. C.P; and J-P T. wrote the manuscript.

Competing Interests: The authors declare no competing financial interests.

References

Aijaz, S., D'Atri, F., Citi, S., Balda, M. S. and Matter, K. (2005). Binding of GEF-H1 to the tight junction-associated adaptor cingulin results in inhibition of Rho signaling and G1/S phase transition. *Dev. Cell* **8**, 777–786.

Bazellières, E., Conte, V., Elosegui-Artola, A., Serra-Picamal, X., Bintanel-Morcillo, M., Roca-Cusachs, P., Muñoz, J. J., Sales-Pardo, M., Guimerà, R. and Trepat, X. (2015). Control of cell-cell forces and collective cell dynamics by the intercellular adhesome. *Nat. Cell Biol.* **17**, 409–20.

Benais-Pont, G., Punn, A., Flores-Maldonado, C., Eckert, J., Raposo, G., Fleming, T. P., Cereijido, M., Balda, M. S. and Matter, K. (2003). Identification of a tight junction-associated guanine nucleotide exchange factor that activates Rho and regulates paracellular permeability. *J. Cell Biol.* **160**, 729–740.

Borghi, N., Sorokina, M., Shcherbakova, O. G., Weis, W. I., Pruitt, B. L., Nelson, W. J. and Dunn, A. R. (2012). E-cadherin is under constitutive actomyosin-generated tension that is increased at cell-cell contacts upon externally applied stretch. *Proc. Natl. Acad. Sci.* **109**, 12568–12573.

Bosveld, F., Markova, O., Guirao, B., Martin, C., Wang, Z., Pierre, A., Balakireva, M., Gaugue, I., Ainslie, A., Christophorou, N., et al. (2016). Epithelial tricellular junctions act as interphase cell shape sensors to orient mitosis. *Nature* **530**, 495–498.

Burkel, B. M., von Dassow, G. and Bement, W. M. (2007). Versatile fluorescent probes for actin filaments based on the actin-binding domain of utrophin. *Cell Motil. Cytoskeleton* **64**, 822–832.

Choi, Y. S., Sehgal, R., McCrea, P. and Gumbiner, B. (1990). A cadherin-like protein in eggs and cleaving embryos of Xenopus laevis is expressed in oocytes in response to progesterone. *J. Cell Biol.* **110**, 1575–82.

Choi, W., Acharya, B. R., Peyret, G., Fardin, M.-A., Mège, R.-M., Ladoux, B., Yap, A. S., Fanning, A. S. and Peifer, M. (2016). Remodeling the zonula adherens in response to tension and the role of afadin in this response. *J. Cell Biol.* **213**, 243–260.

Citi, S., Guerrera, D., Spadaro, D. and Shah, J. (2014). Epithelial junctions and Rho family GTPases: the zonular signalosome. *Small GTPases* **1248**, 37–41.

Dejana, E., Tournier-Lasserve, E. and Weinstein, B. M. (2009). The Control of Vascular Integrity by Endothelial Cell Junctions: Molecular Basis and Pathological

Implications. *Dev. Cell* **16**, 209–221.

Fanning, A. S., Jameson, B. J., Jesaitis, L. A. and Anderson, J. M. (1998). The tight junction protein ZO-1 establishes a link between the transmembrane protein occludin and the actin cytoskeleton. *J. Biol. Chem.* **273**, 29745–53.

Fanning, a. S., Van Itallie, C. M. and Anderson, J. M. (2012). Zonula occludens-1 and -2 regulate apical cell structure and the zonula adherens cytoskeleton in polarized epithelia. *Mol. Biol. Cell* **23**, 577–590.

Founounou, N., Loyer, N. and Le Borgne, R. (2013). Septins Regulate the Contractility of the Actomyosin Ring to Enable Adherens Junction Remodeling during Cytokinesis of Epithelial Cells. *Dev. Cell* **24**, 242–255.

Fujiwara, T., Bandi, M., Nitta, M., Ivanova, E. V., Bronson, R. T. and Pellman, D. (2005). Cytokinesis failure generating tetraploids promotes tumorigenesis in p53-null cells. *Nature* **437**, 1043–1047.

Furuse, M., Itoh, M., Hirase, T., Nagafuchi, A., Yonemura, S., Tsukita, S. and Tsukita, S. (1994). Direct association of occludin with ZO-1 and its possible involvement in the localization of occludin at tight junctions. *J. Cell Biol.* **127**, 1617–26.

Ginsberg, D., DeSimone, D. and Geiger, B. (1991). Expression of a novel cadherin (EP-cadherin) in unfertilized eggs and early Xenopus embryos. *Development* **111**, 315–25.

Grashoff, C., Hoffman, B. D., Brenner, M. D., Zhou, R., Parsons, M., Yang, M. T., McLean, M. A., Sligar, S. G., Chen, C. S., Ha, T., et al. (2010). Measuring mechanical tension across vinculin reveals regulation of focal adhesion dynamics. *Nature* **466**, 263–6.

Guillot, C. and Lecuit, T. (2013). Adhesion Disengagement Uncouples Intrinsic and Extrinsic Forces to Drive Cytokinesis in Epithelial Tissues. *Dev. Cell* **24**, 227–241.

Guilluy, C., Swaminathan, V., Garcia-Mata, R., O'Brien, E. T., Superfine, R. and Burridge, K. (2011). The Rho GEFs LARG and GEF-H1 regulate the mechanical response to force on integrins. *Nat. Cell Biol.* **13**, 722–727.

Hatte, G., Tramier, M., Prigent, C. and Tassan, J.-P. (2014). Epithelial cell division in the Xenopus laevis embryo during gastrulation. *Int. J. Dev. Biol.* **58**, 775–781.

Herbomel, G., Hatte, G., Roul, J., Padilla-Parra, S., Tassan, J.-P. and Tramier, M. (2017). Actomyosin-generated tension on cadherin is similar between dividing and non-dividing epithelial cells in early Xenopus laevis embryos. *Sci. Rep.* **7**, 45058.

Herszterg, S., Leibfried, A., Bosveld, F., Martin, C. and Bellaiche, Y. (2013). Interplay between the Dividing Cell and Its Neighbors Regulates Adherens Junction Formation during Cytokinesis in Epithelial Tissue. *Dev. Cell* **24**, 256–270.

Higashi, T., Arnold, T. R., Stephenson, R. E., Dinshaw, K. M. and Miller, A. L. (2016). Maintenance of the Epithelial Barrier and Remodeling of Cell-Cell Junctions during Cytokinesis. *Curr. Biol.* **26**, 1829–1842.

Itoh, K., Ossipova, O. and Sokol, S. Y. (2014). GEF-H1 functions in apical constriction and cell intercalations and is essential for vertebrate neural tube closure. *J Cell Sci* **127**, 2542–2553.

Krendel, M., Zenke, F. T. and Bokoch, G. M. (2002). Nucleotide exchange factor GEF-H1 mediates cross-talk between microtubules and the actin cytoskeleton. *Nat. Cell Biol.* **4**, 294–301.

Le Page, Y., Chartrain, I., Badouel, C. and Tassan, J.-P. (2011). A functional analysis of MELK in cell division reveals a transition in the mode of cytokinesis during Xenopus development. *J. Cell Sci.* **124**, 958–968.

Leckband, D. E. and de Rooij, J. (2014). Cadherin adhesion and mechanotransduction. *Annu. Rev. Cell Dev. Biol.* **30**, 291–315.

Lecuit, T. and Yap, A. S. (2015). E-cadherin junctions as active mechanical integrators in tissue dynamics. *Nat. Cell Biol.* **17**, 533–9.

Leray, A., Padilla-Parra, S., Roul, J., Héliot, L. and Tramier, M. (2013). Spatio-Temporal Quantification of FRET in living cells by fast time-domain FLIM: a comparative study of non-fitting methods [corrected]. *PLoS One* **8**, e69335.

Marx, A., Godinez, W. J., Tsimashchuk, V., Bankhead, P., Rohr, K. and Engel, U. (2013). Xenopus cytoplasmic linker-associated protein 1 (XCLASP1) promotes axon elongation and advance of pioneer microtubules. *Mol. Biol. Cell* **24**, 1544–1558.

Matsuda, M. (2004). A peculiar internalization of claudins, tight junction-specific adhesion molecules, during the intercellular movement of epithelial cells. *J. Cell Sci.* **117**, 1247–1257.

Morais-de-Sá, E. and Sunkel, C. (2013). Adherens junctions determine the apical position of the midbody during follicular epithelial cell division. *EMBO Rep.* **14**, 696–703.

Nandadasa, S., Tao, Q., Shoemaker, A., Cha, S. wook and Wylie, C. (2012). Regulation of classical cadherin membrane expression and F-actin assembly by alpha-catenins,

during Xenopus embryogenesis. *PLoS One* **7**,.

Pathak, R., Delorme-Walker, V. D., Howell, M. C., Anselmo, A. N., White, M. A., Bokoch, G. M. and DerMardirossian, C. (2012). The Microtubule-Associated Rho Activating Factor GEF-H1 Interacts with Exocyst Complex to Regulate Vesicle Traffic. *Dev. Cell* **23**, 397–411.

Regnier, M., Rivera, A. J., Chen, Y. and Chase, P. B. (2000). 2-deoxy-ATP enhances contractility of rat cardiac muscle. *Circ. Res.* **86**, 1211–7.

Reyes, C. C., Jin, M., Breznau, E. B., Espino, R., Delgado-Gonzalo, R., Goryachev, A. B. and Miller, A. L. (2014). Anillin regulates cell-cell junction integrity by organizing junctional accumulation of Rho-GTP and actomyosin. *Curr. Biol.* **24**, 1263–70.

Stevenson, B. R., Siliciano, J. D., Mooseker, M. S. and Goodenough, D. A. (1986). Identification of ZO-1: a high molecular weight polypeptide associated with the tight junction (zonula occludens) in a variety of epithelia. *J. Cell Biol.* **103**, 755–66.

Tornavaca, O., Chia, M., Dufton, N., Almagro, L. O., Conway, D. E., Randi, A. M., Schwartz, M. A., Matter, K. and Balda, M. S. (2015). ZO-1 controls endothelial adherens junctions, cell-cell tension, angiogenesis, and barrier formation. *J. Cell Biol.* **208**, 821–38.

Twiss, F. and de Rooij, J. (2013). Cadherin mechanotransduction in tissue remodeling. *Cell. Mol. Life Sci.* **70**, 4101–16.

Wu, B. and Guo, W. (2015). The Exocyst at a Glance. *J. Cell Sci.* **128**, 2957–64.

Yao, M., Qiu, W., Liu, R., Efremov, A. K., Cong, P., Seddiki, R., Payre, M., Lim, C. T., Ladoux, B., Mège, R.-M., et al. (2014). Force-dependent conformational switch of α-catenin controls vinculin binding. *Nat. Commun.* **5**, 4525.

Yonemura, S., Wada, Y., Watanabe, T., Nagafuchi, A. and Shibata, M. (2010). α-Catenin as a tension transducer that induces adherens junction development. *Nat. Cell Biol.* **12**, 533–542.

Figures

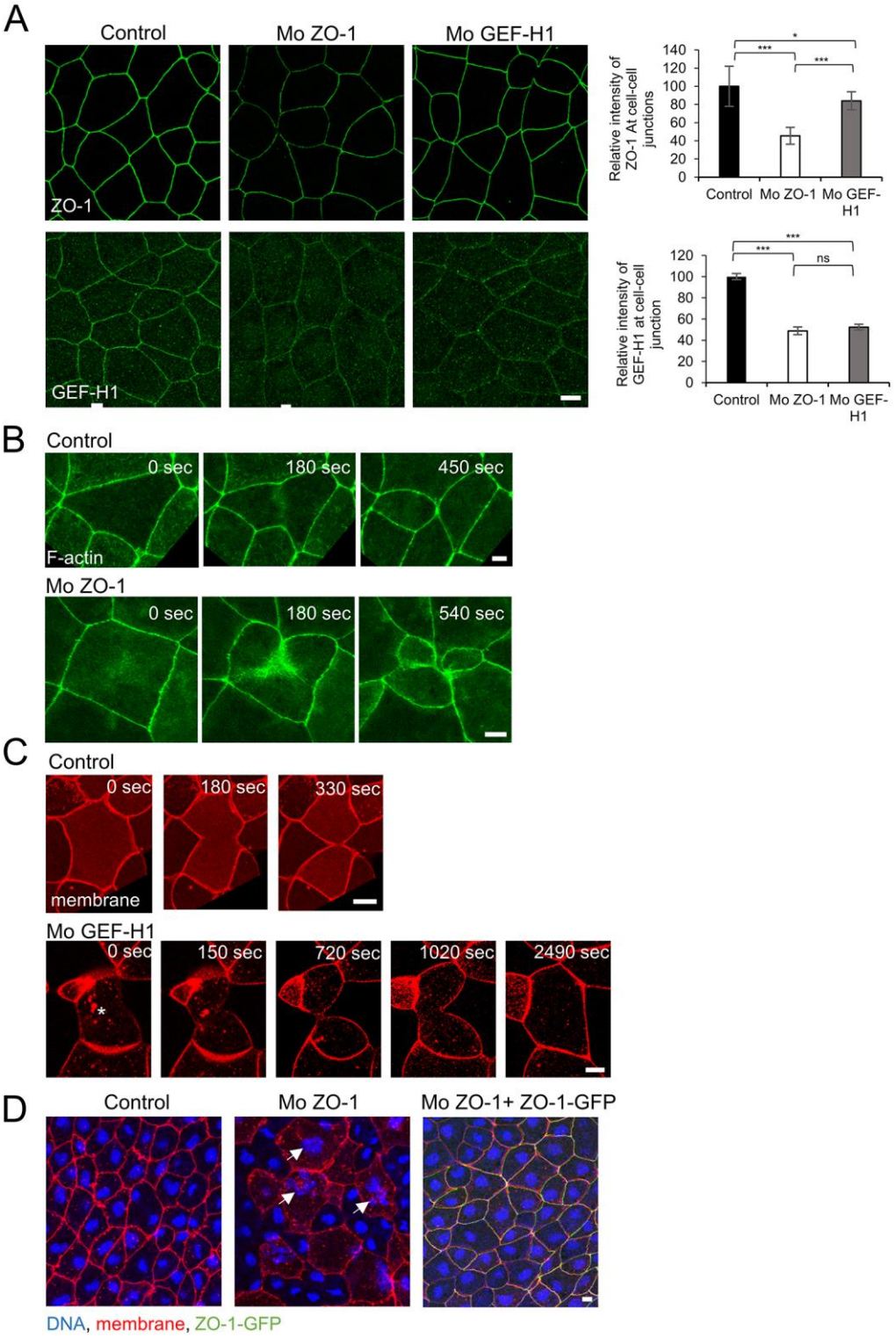

Figure 1: ZO-1 and GEF-H1 depletions lead to cytokinesis defects

(A) Endogenous ZO-1 and GEF-H1 proteins in untreated (control), ZO-1 depleted (Mo ZO-1) and GEF-H1 depleted (Mo GEF-H1) embryos. Images are maximal projections. Relative intensities of endogenous ZO-1 and GEF-H1 proteins at cell-cell junctions in control, ZO-1 depleted (Mo ZO-1) and GEF-H1 depleted (Mo GEF-H1) cells are presented on histograms on the right.

(B) Still images extracted from time lapse of control and ZO-1 depleted cells expressing a fluorescent F-actin probe. The ZO-1 depleted cell exhibits multiple cytokinetic furrows.

(C) Still images extracted from time lapse of control and GEF-H1 depleted cells traced with RFP-membrane. Cell marked by an asterisk fails to divide.

(D) ZO-1 depletion in Xenopus gastrulae. Injected cells were traced with membrane marker (red) and DNA was stained with topro3 (blue). Mouse ZO-1-GFP, resistant to Mo ZO-1 (due to the divergence of its nucleotide sequence with the Xenopus sequence), expressed in ZO-1 depleted cells traced with membrane marker (Mo ZO-1 + ZO-1-GFP). Arrows point to multinucleated cells. Proportion of embryos exhibiting multinucleated cells: control 4.5% n=22 embryos analysed, Mo ZO-1 79.6% n=23 and Mo ZO-1 + ZO-1-GFP 17.4% n=23.

Data represent means ± s.e.m. ns: not significant, * =$p<0.05$, *** =$p<0.0001$. Scale bars, 10 µm.

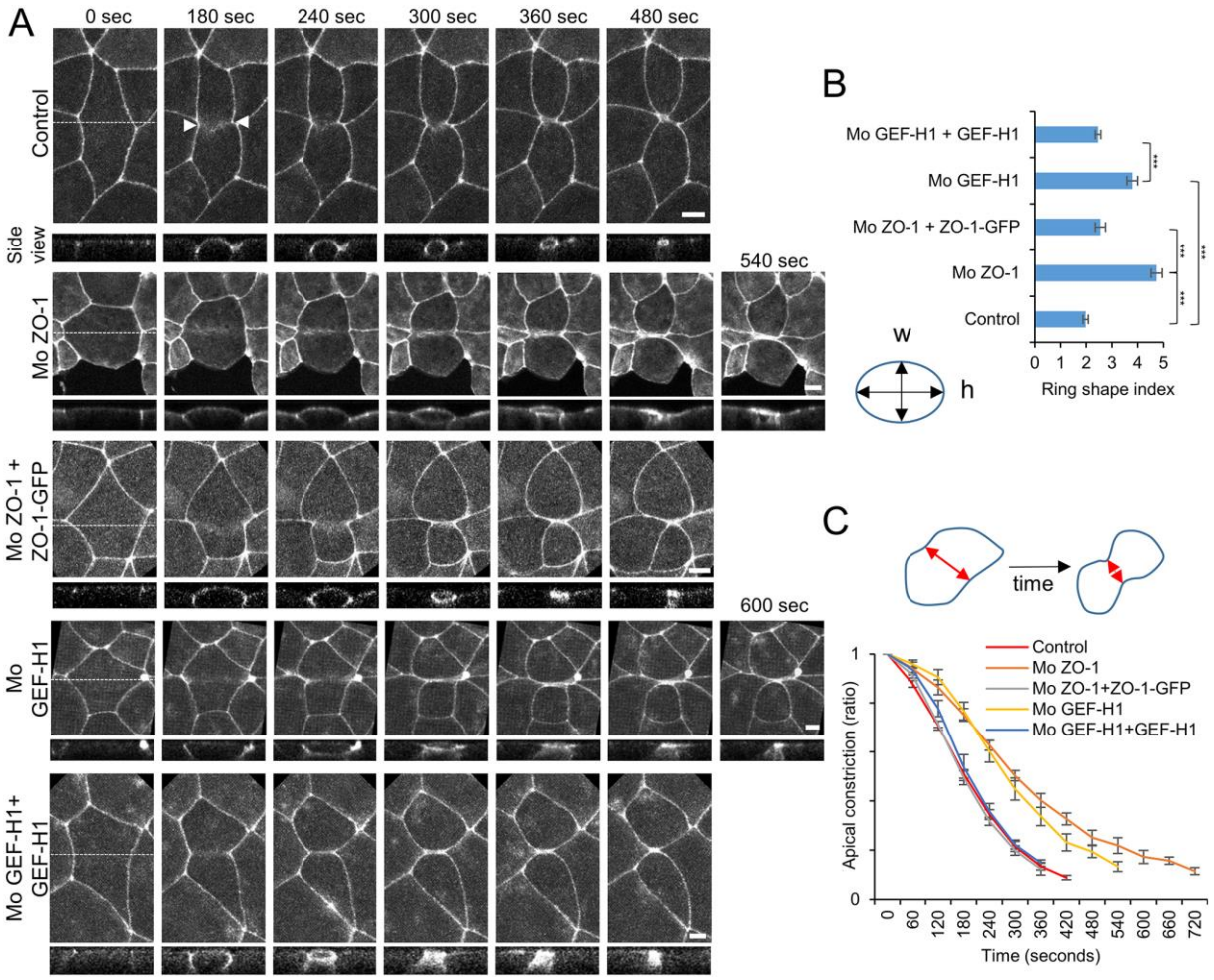

Figure 2: Tight junctions are essential during cytokinesis.

(A) Still images extracted from time lapse of dividing cells expressing fluorescent F-actin probes alone (control) or in Zo-1 depleted (Mo ZO-1), ZO-1 depleted expressing ZO-1-GFP (Mo ZO-1 + ZO-1 GFP), GEF-H1 depleted (Mo GEF-H1) and GEF-H1 depleted expressing GEF-H1 (Mo GEF-H1 + GEF-H1) embryos. Maximal projections of en face views and side views parallel to the cleavage plane through the contractile ring are shown. Cells shown are representative of 46/46 recorded cells for the control (100%), 21/21 for Mo ZO-1 (100%), 10/13 for Mo ZO-1 + ZO-1-GFP (77%), 13/22 for Mo GEF-H1 (59.1%) and 16/26 for Mo GEF-H1 + GEF-H1 (61.5%).

(B) Contractile ring shape index (R.S.I.) in conditions shown in a. The oval represents the contractile ring, w: width, h: height. Control: 2.1 ± 0.1 (mean ± s.e.m.) n=46 cells, Mo ZO-1: 4.7 ± 0.2 n=21, Mo ZO-1 + ZO-1-GFP: 2.5 ± 0.1 n=10, Mo GEF-H1: 3.8 ± 0.2 n=13, Mo GEF-H1 + GEF-H1: 2.4 ± 0.1 n=16.

(C) Apical constriction at the cleavage site in conditions shown in **(a)**. The red arrow represents the distance separating plasma membranes at the division site measured over time. Control: 377.5 ± 11.4 s, Mo ZO-1: 648 ± 45.1 s, Mo ZO-1 + ZO-1-GFP: 370±10 s, Mo GEF-H1: 538 ± 27.6 s, Mo GEF-H1 + GEF-H1: 384±6 s.

Data represent means ± s.e.m.. * = $p<0.05$, *** =$p<0.0001$. Scale bars, 10 µm.

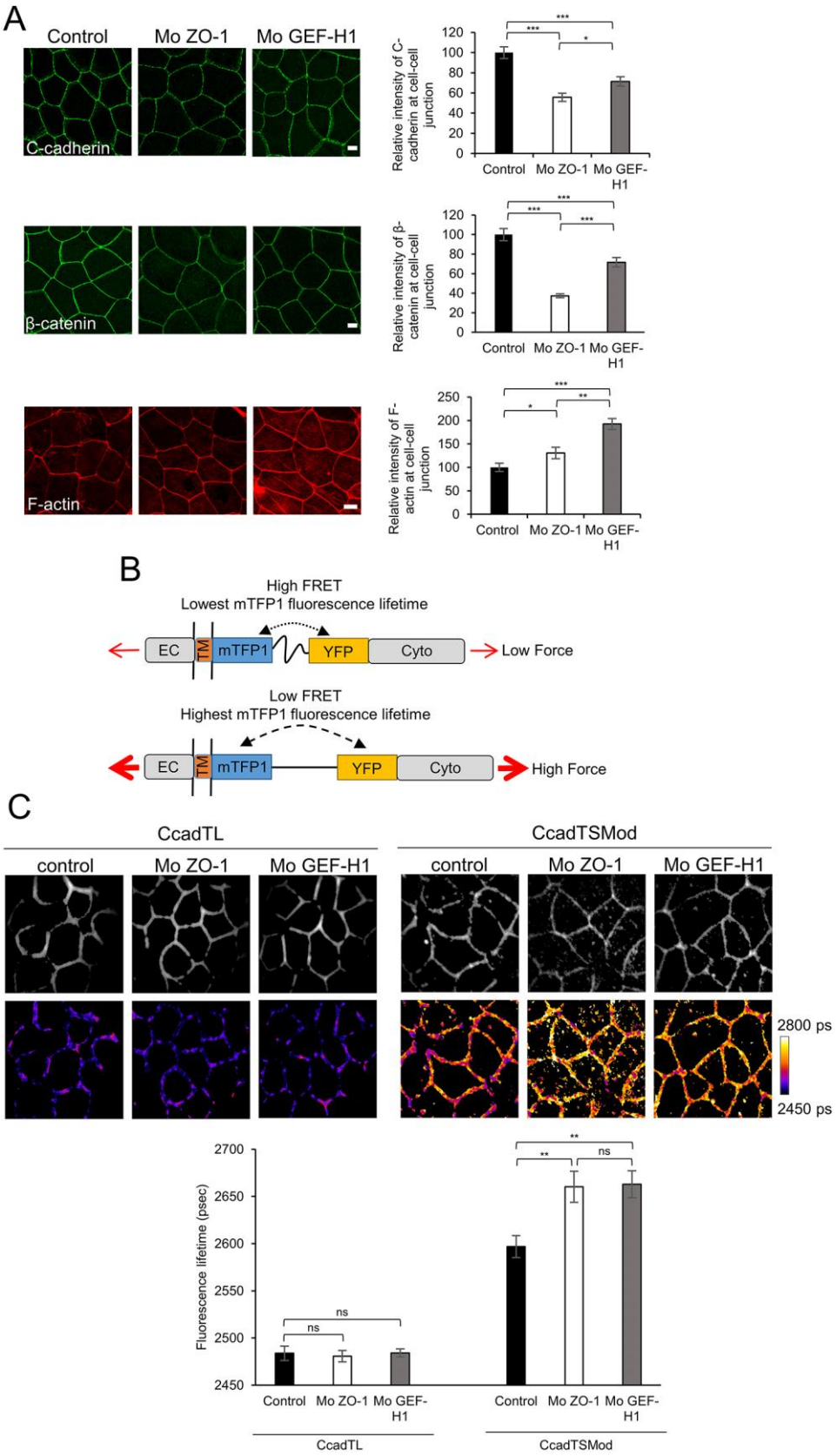

Figure 3: ZO-1 and GEF-H1 regulate tension applied to adherens junctions.

(A) Endogenous C-cadherin, β-catenin and F-actin in control, ZO-1 depleted (Mo ZO-1) and GEF-H1 depleted (Mo GEF-H1) cells. Maximal projections of confocal sections are shown. Graphs: relative intensity of each protein at cell-cell junctions in control and depleted cells. C-cadherin: 55.7 % ± 4.1 % in Mo ZO-1 and 71.7% ± 4.7 % in Mo GEF-H1, β-catenin: 37.3 % ± 2.1 % in Mo ZO-1 and 71.4 % ± 4.7 % in Mo GEF-H1, F-actin: 130.6 % ± 12.2 % in Mo ZO-1 cells and 192.5 % ± 11.6 % in Mo GEF-H1.

(B) Schematic representation of the CcadTSMod biosensor. The relation between the FRET and donor fluorescence lifetime being inverse, in absence of tension (top, the tension sensor module (TSMod, black line) is not elongated), FRET is high and fluorescence lifetime is low. Reversely, in presence of tension (bottom, the TSMod is elongated), FRET decreases and the donor fluorescence lifetime increases. EC, Cyto and TM: respectively extracellular, cytoplasmic and transmembrane domains of C-cadherin.

(C) Tensile forces applied to adherens junctions in control, ZO-1 depleted (Mo ZO-1) and GEF-H1 depleted (Mo GEF-H1) cells expressing CcadTL or the CcadTSMod biosensor. Top panel: representative images of mTFP1 fluorescence (upper row images) and the corresponding fluorescence lifetimes (bottom row images) are shown. The pseudocolour scale represents pixel-by-pixel fluorescence lifetime expressed in ps. Bottom panel: graph of mean fluorescence lifetime of CcadTL and CcadTSMod tension probe at the cell-cell contacts in control (n=25 and 29 fields respectively), ZO-1 depleted (n=29 and 19 fields) and GEF-H1 depleted (n=41 and 22 fields) cells. Data are representative of 3 independent experiments.

Data represent means ± s.e.m.. * = $p<0.05$, ** =$p<0.001$, *** =$p<0.0001$. Scale bars, 10 µm.

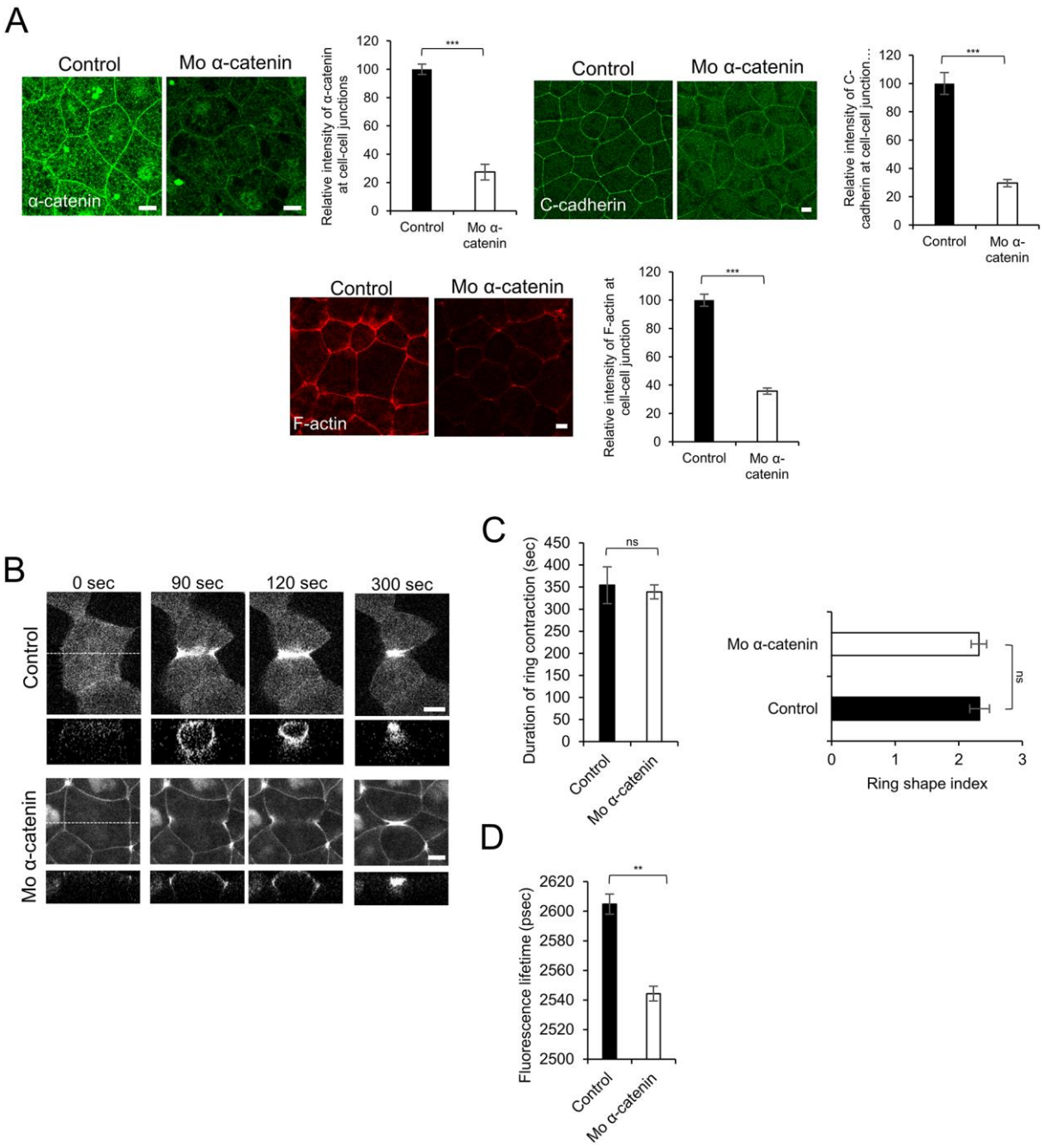

Fig. 4: unaltered cytokinesis in α-catenin depleted cells

(A) Images: endogenous α-catenin, C-cadherin and F-actin in control and embryos treated with α-catenin morpholino (Nandadasa et al., 2012). Histogram on the right: relative fluorescence intensities for each protein at cell-cell contacts. α-catenin: 27.4 ± 5.5 % of controls, C-cadherin: 29.6 ± 2.5 % and F-actin: 35.8 ± 2.2.

(B) Still images from time lapse movies of dividing control and α-catenin depleted (Mo α-catenin) cells expressing fluorescent lifeact F-actin probe. Maximal projections and side views parallel to the cleavage plane are presented. Control: 17 out of 17 recorded cells (100 %), Mo α-catenin: 17 out of 19 recorded cells (89.5 %).

(C) Left: cytokinesis duration in control and α-catenin depleted cells. Control: 354±41.6 s, Mo α-catenin: 339 ± 16.1 s. Right: ring shape index in control and α-catenin depleted cells. Control: 2.1 ± 0.1, Mo α-catenin: 2.3 ± 0.1.

(D) Variation of fluorescence lifetimes of the CcadTSMod tension probe in control cells or α–catenin depleted cells. Control n=8 fields, Mo α-catenin n=32 fields

Data represent means ± s.e.m.. ns: not significant, *** =p<0.0001,. Scale bars, 10 μm

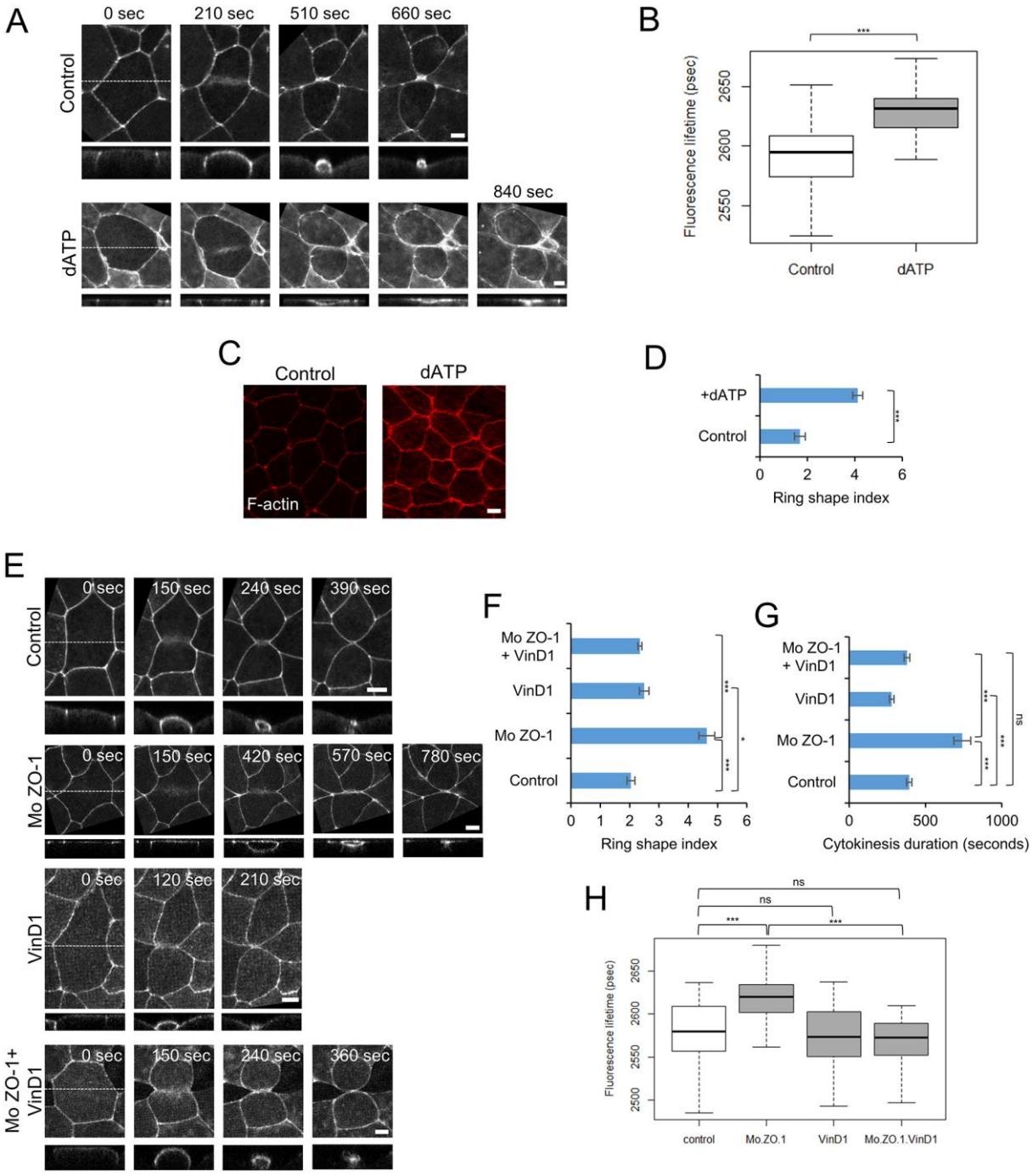

Figure 5: Increased tensile forces applied on adherens junctions induces cytokinesis defects

(A) Still images from time lapse movies of dividing cells expressing fluorescent lifeact F-actin probe in embryos treated with dATP or not (control).

(B) Boxplot of mean fluorescence lifetimes (in psec) of the CcadTSMod tension probe at cell-cell contacts in controls (2590.3 ±6.6 ps, n=23 fields) and dATP treated (2627.1 ± 4.7 ps, n=24 fields) cells.

(C) Endogenous F-actin in control and dATP treated embryos.

(D) Ring shape index and cytokinesis duration in control and dATP treated cells. Control: R.S.I. : 1.7 ± 0.2 n=12 cells , duration : 620 ± 21.2 s n=9, +dATP: R.S.I. : 4.1 ± 0.2 n=32, duration : 772 ± 103.7 s n=8.

(E) Still images extracted from time lapse of dividing cells expressing fluorescent lifeact F-actin probe alone (control) or in ZO-1 depleted (Mo ZO-1), VinD1 expressing (VinD1) and ZO-1 depleted and expressing VinD1 (Mo ZO-1 + VinD1) embryos. For each condition, maximal projections of en face views (upper row images) and side views (lower row images) parallel to the cleavage plane through the contractile ring at are shown. Controls 26/26 of recorded cells (100 %), Mo ZO-1: 21/23 (91.3 %), VinD1: 8/10 (80%), Mo ZO-1 + VinD1: 26/39 (66.7%).

(F) Ring shape index and **(G)** cytokinesis duration in control, ZO-1 depleted (Mo ZO-1), VinD1 expressing (VinD1) and ZO-1 depleted and expressing VinD1 (Mo ZO-1 + VinD1) cells. Controls n=21 cells, Mo ZO-1 n= 10 cells, VinD1 n=16 cells, Mo ZO-1 + VinD1 n=21 cells.

(H) Tensile forces applied to adherens junctions in control, ZO-1 depleted, and ZO-1 depleted and expressing VinD1 (Mo ZO-1 + VinD1) cells. Boxplot of mean fluorescence lifetimes of the CcadTSMod tension probe at cell-cell contacts in control (2579 ± 5.1 ps, n=47 fields), ZO-1 depleted (Mo ZO-1, 2618.3 ± 5.6 ps, n=29 fields), VinD1 expressing (VinD1, 2576.6 ± 6.8 ps, n=26 fields) cells and ZO-1 depleted and expressing VinD1 (Mo ZO-1 + VinD1, 2566.0 ± 8.4 ps, n=16 fields).

Data represent means ± s.e.m.. ns: not significant, * =$p<0.05$, ** = $p<0.001$, *** =$p<0.0001$. Scale bars, 10 μm.

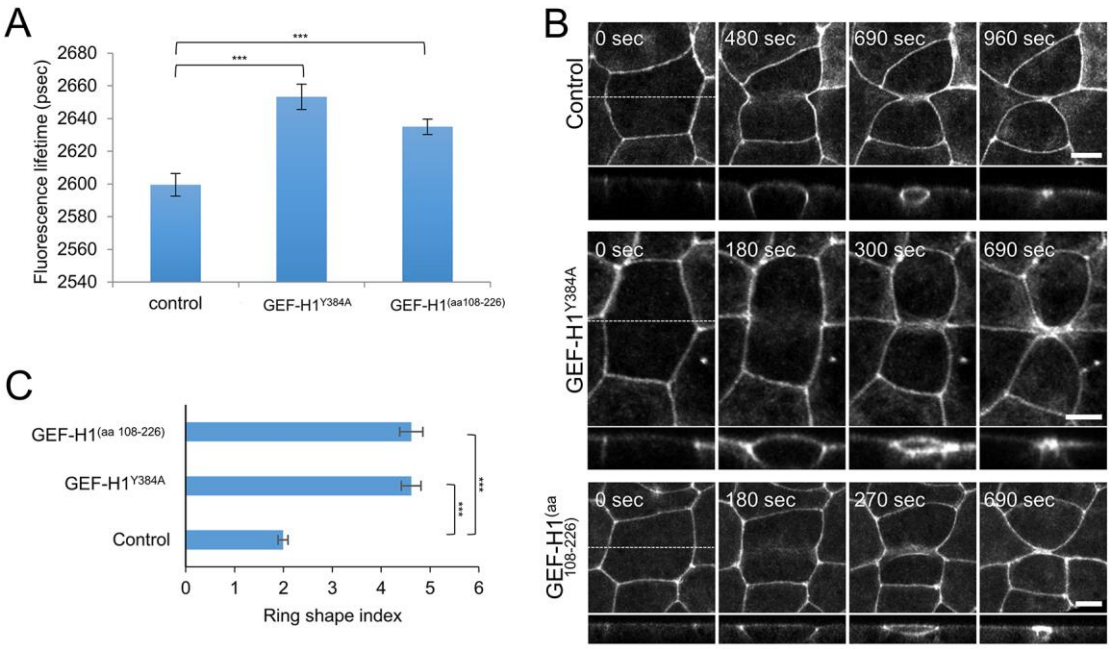

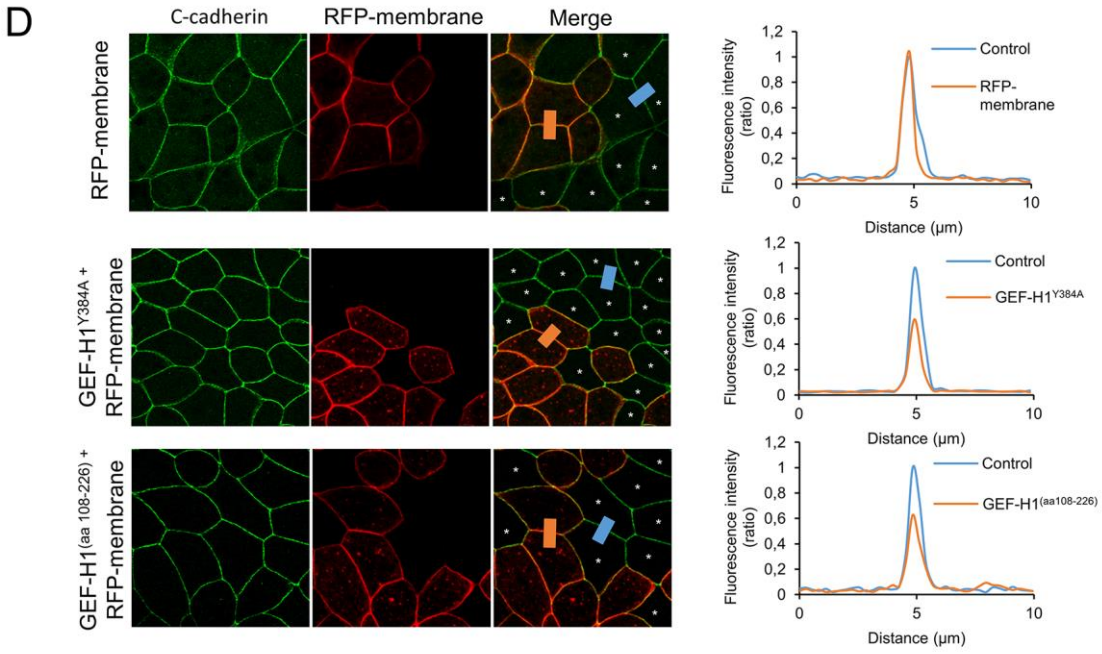

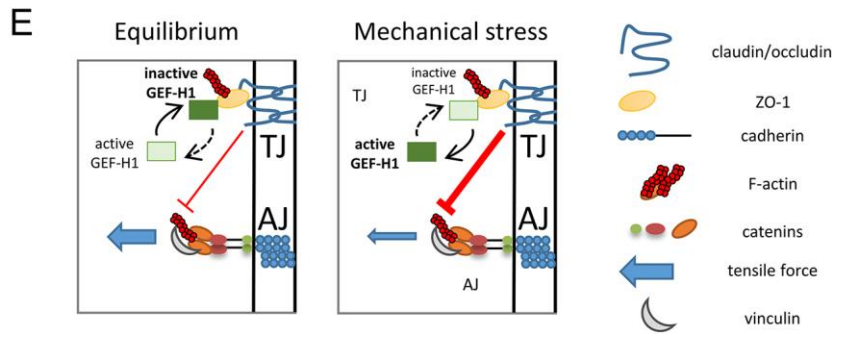

Figure 6: Involvement of GEF-H1 activity and potential interaction with the exocyst complex in the regulation of tensile forces applied on adherens junctions

(A) Variation of fluorescence lifetimes of the CcadTSMod tension probe in cells expressing mutants used in (A): GEF-H1^{Y384A} (n=28 fields) and GEF-H1$^{(aa\ 108\text{-}226)}$ (n=35). Data are representative of 3 independent experiments.

(B) Still images extracted from time lapse movies of cells expressing a fluorescent F-actin probe only (control, 100% of recorded cells, n=38) or coexpressing GEF-H1^{Y384A} (100%, n=12 cells), GEF-H1$^{(aa108\text{-}226)}$ (69%, n=42),

(C) Ring shape index in control (2.0 ± 0.1, n=38 cells), GEF-H1^{Y384A} (4.6 ± 0.2, n=12) and GEF-H1$^{(aa\ 108\text{-}226)}$ (4.6 ± 0.2, n=29) expressing cells.

(D) Left, endogenous C-cadherin, in control, GEF-H1^{Y384A} and GEF-H1$^{(aa\ 108\text{-}226)}$ expressing cells. The co-expression of RFP-membrane was used as a tracer. For each condition, an image of a field containing cells expressing and not expressing RFP-membrane is shown. Cells, which do not express RFP-membrane are used as internal control for fluorescence quantifications. Red and blue lines on merge images indicate cell-cell contacts where fluorescence was quantified. Right, line scans show C-cadherin intensity in internal control (blue) and cells expressing the RFP-membrane (red) in each condition. Cells, which do not express RFP-membrane are marked by the asterisks. See also supplementary material Fig. S3.

(E) Model of the regulation by tight junctions of tensile forces applied to adherens junctions. The two tight junction-associated proteins ZO-1 and GEF-H1 are involved in the regulation of mechanical forces applied to adherens junctions. When tensile forces are at the equilibrium, GEF-H1 is inhibited by junctional recruitment (Aijaz et al. 2005) and the inhibition (exerted by tight junctions (TJ)) of mechanical forces applied on adherens junctions is low. Under mechanical stress, such as cytokinesis, GEF-H1 would be released from junctional inhibition. Active GEF-H1 would trigger, at the tight junctions level, a response leading to increased inhibition of mechanical forces applied on adherens junctions (AJ).

Data represent means ± s.e.m.. *** =$p<0.0001$. Scale bars, 10 µm.

Supplementary Material: supplementary figure 1-3

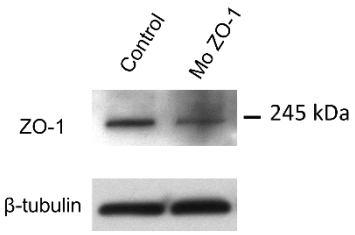

Fig. S1: Immunoblot showing knockdown of endogenous ZO-1. Proteins were extracted from control and Mo ZO-1 injected embryos and blotted with anti-ZO-1 antibody. β-tubulin was used as a loading control.

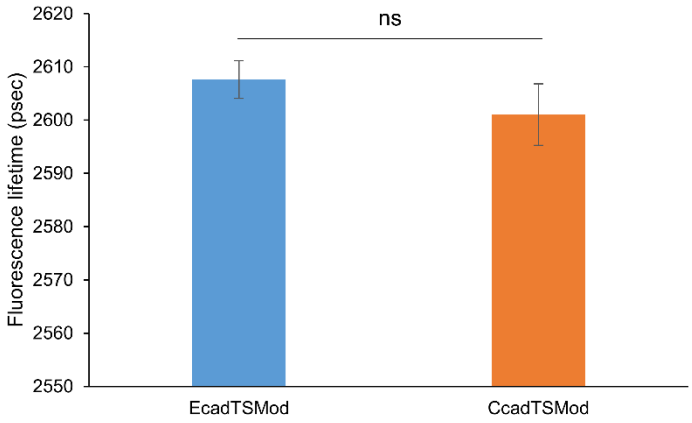

Fig. S2: Boxplot of EcadTSMod and CcadTSMod mean fluorescence lifetimes at gastrula stage. n= 29 and 31, respectively. ns: not significant.

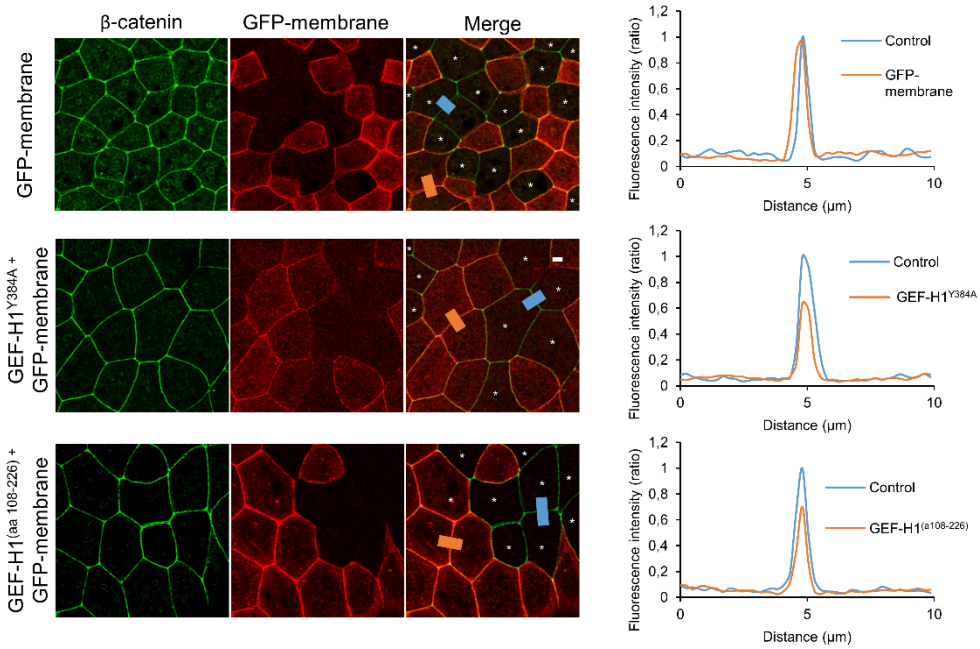

Fig. S3: Left, endogenous β-catenin, in control, GEF-H1^{Y384A} and GEF-H1$^{(aa\ 108\text{-}226)}$ expressing cells. The co-expression of GFP-membrane was used as a tracer. For each condition, an image of a field containing cells expressing and not expressing RFP-membrane is shown. Cells, which do not express RFP-membrane are used as internal controls for fluorescence quantifications. Red and blue lines on merge images indicate cell-cell contacts where fluorescence was quantified. Right, line scans show β-catenin fluorescence intensity in internal control (blue line) and cells expressing the GFP-membrane (red line) in each condition. Cells which do not express GFP-membrane are marked by asterisks. Scale bars, 10 μm.